

**Monoatomic and dimer Mn adsorption on the Au(111) surface from first principles**Francisco Muñoz,<sup>1,2</sup> Aldo H. Romero,<sup>3</sup> Jose Mejía-López,<sup>1,2</sup> and J. L. Morán-López<sup>4</sup><sup>1</sup>*Departamento de Física, Facultad de Ciencias, Universidad Nacional Autónoma de México, México D.F. México*<sup>2</sup>*Centro para el Desarrollo de la Nanociencia y la Nanotecnología CEDENNA, Avda. Ecuador 3493, Santiago, Chile*<sup>3</sup>*CINVESTAV, Unidad Querétaro, Libramiento Norponiente 2000, Real de Juriquilla, CP 76230, Querétaro, México*<sup>4</sup>*Departamento de Física, Facultad de Ciencias, Universidad Nacional Autónoma de México (UNAM), México D. F. México*

(Received 9 December 2010; revised manuscript received 14 March 2011; published 23 May 2011)

A theoretical study based on the density functional theory of the adsorption of Mn monomers and dimers on a Au-(111) surface is presented. As necessary preliminary steps, the bulk and clean surface electronic structure are calculated, which agree well with previous reports. Then, the electronic structure of the Mn adatom, chemisorbed on four different surface geometries, is analyzed. It is found that the most stable geometry is when the Mn atom is chemisorbed on threefold coordinated sites. Using this geometry for a single adatom a second Mn atom is chemisorbed and the most stable dimer geometrical structure is calculated. The lowest-energy configuration corresponds to the molecule lying parallel to the surface, adsorbed on two topological equivalent threefold coordinated sites. It is also found that the lowest-energy magnetic configuration corresponds to the antiferromagnetic arrangement with individual magnetic moments of  $4.64\mu_B$ . Finally, it is concluded that the dimer is not stable and should fragment at the surface.

DOI: [10.1103/PhysRevB.83.205423](https://doi.org/10.1103/PhysRevB.83.205423)

PACS number(s): 34.35.+a, 75.70.Rf, 31.10.+z, 31.15.A-

**I. INTRODUCTION**

Most of the foreseen technological applications of nanostructures imply the deposition of well-characterized nanoparticles, or thin films, on particular substrates. Thus, after a full characterization of free clusters and of the chosen substrate, it is imperative to know the changes introduced by the substrate-cluster interactions. In particular, the growth of ultrathin films or nanostructures based on magnetic transition metals and deposited on different substrates has been the subject of intensive research,<sup>1-6</sup> but the effect of the substrate-nanostructure interactions is not fully understood.

Depending on the substrate-adatom interaction, one may expect important modifications to the magnetic properties of the transition-metal adatoms and perhaps the appearance of new magnetic phases in structures adsorbed on nonmagnetic substrates. One of the systems that has garnered much attention is the adsorption of Mn on metallic surfaces because of the following: (i) Mn is the transition metal with the highest atomic magnetic moment ( $5\mu_B$ ) and can be used to deposit overlayers of ferromagnetically coupled atoms which could lead to technological applications, (e.g., spintronics<sup>7</sup>). (ii) A fundamental motivation is to understand the interplay between the different orbitals on the bonding process to metallic substrates. In general, it is expected that after adsorption, the bonding and hybridization would decrease the atomic magnetic moment, unless charge transfer from the surface to the majority-spin levels compensates that reduction. (iii) Recent calculations on free Mn dimers show that the magnetic coupling depends on the distance between the two atoms.<sup>8</sup> The ferromagnetic (FM) and antiferromagnetic (AFM) configurations are stable above and below 3.06 Å, respectively. The ground state is the AFM arrangement with a bond distance of 2.89 Å. Although chemisorption may produce many changes in the electronic structure of the deposited species, it is interesting to see if under chemisorption, on particular substrates and surface orientations, the dimer bond length can be modified and induce one coupling or the other. As mentioned above, due

to the high atomic Mn magnetic moment, it is interesting to find out whether under particular circumstances ferromagnetic coupled nanostructures or thin films can be generated.

It is well known that Mn in bulk samples presents a rich variety of magnetic behaviors, which depend on crystalline structure, temperature, and pressure.<sup>9</sup> Thanks to that, a complex behavior is observed in small clusters, where the average magnetic moment shows a non-monotonic size dependence.<sup>10</sup> The theoretical results by Mejía *et al.*<sup>8,11</sup> on very small clusters offer as a possible explanation for such behavior. They propose that complex noncollinear structures are produced due to the AFM interactions between nearest neighbors and the ferromagnetic interactions among more distant pairs. Thus, it is of great relevance to study the changes on the magnetic properties, of multiatom clusters, induced by the adsorption process.

Experimentally it has been observed that the growth of Mn on noble-metal substrates has the following characteristics: For low coverage the adatoms remain at the surface on particular sites. Upon increasing the coverage, there is a tendency to exchange sites between the topmost surface atoms and Mn, forming a surface alloy. Further deposition leads to Mn islands. This growth mechanism has been observed, by scanning tunneling microscopy (STM), on Cu(100),<sup>12</sup> Cu(110),<sup>13</sup> Ag(100),<sup>14</sup> and Au(111)<sup>15</sup> surfaces.

From a theoretical point of view, several *ab initio* and semiempirical calculations have found, in addition to the FM and AFM arrangements, noncollinear magnetic behavior in both supported<sup>16</sup> and free Mn clusters.<sup>8,17</sup> There is a general consensus that Mn clusters supported on a metal surface develop noncollinear ordering due mainly to frustration in the AFM order.<sup>18</sup> Another feature observed on small Mn clusters when deposited on some specific metal surfaces is magnetic bistability, where, due to an almost degenerate ground-state energy, there is a coexistence of both FM and AFM ordering.<sup>19</sup> Finally, it is important to note that most theoretical studies of Mn clusters supported on noble metals neglect a proper

structural optimization of the substrate, mainly due to high computational costs. Nevertheless, we are convinced that a clear interpretation of the chemisorption process of a single adatoms or dimers of molecules, including the structure optimization, is of vital importance in understanding the growth and properties of larger nanostructures.

Here, we report a set of total energy calculations of the adsorption of Mn adatoms and dimers on Au(111) surfaces. We calculate the electron density distribution, the magnetic moment, and the bond lengths at various chemisorption sites. In Sec. II a brief description of the computational approach is presented. Then, in Sec. III, we discuss the clean Au(111) surface properties and compare our findings with results previously reported in the literature. The energetics and structure of a single Mn atom adsorption on the Au surface are presented in Sec. IV. The results on the adsorption of the Mn dimer are contained in Sec. V. Finally, we discuss our results and present the conclusions in Sec. VI.

## II. COMPUTATIONAL METHODS

We performed a density functional theory (DFT)<sup>20</sup> study as implemented within the framework of the Vienna *Ab-initio* Simulation Package (VASP).<sup>21–24</sup> We consider only valence electrons and describe them with projector-augmented-wave (PAW) types of pseudopotentials<sup>25,26</sup> to take into account spin-orbit interactions (SOIs). It is worth noticing that although SOIs in the manganese atoms are important, as compared to other noble metals, they are much smaller than the SOIs in Au atoms and influence only to a small extent our numerical results. For the exchange correlation we use the Perdew-Burke-Ernzerhof (PBE) description.<sup>27</sup> The energy cutoff for the plane waves was set at 260 eV in all calculations. This value assures a force convergence of less than 0.01 eV/Å.

Our study started by testing the exactness of the assumptions and approximations made. For that purpose, we started by calculating the ground-state electronic structure of bulk gold. As a result, we found that Au crystallizes with a fcc geometry with a lattice parameter of 4.17 Å, a value that compares well with the experimental one, 4.08 Å.<sup>28</sup> We also noticed that the calculated electronic structure reproduces very well previous reports. With the confidence that our approximation describes the bulk system well, next we calculated the electronic structure of the Au(111) surface. We modeled the surface region as a slab of five layers; two of them were kept fixed to the bulk parameters and the other three were allowed to relax. After the total relaxation of the atomic positions of the three topmost layers we found that the surface layer expands 2%, and the second one compresses 0.8%. This behavior also compares well with the reported experimental values of 3.3% and 1%, respectively.<sup>29</sup> It is well documented that the Au (111) surface reconstructs with a long periodicity,<sup>29,30</sup> and its simulation requires to consider a  $(22 \times \sqrt{3})$  cell.<sup>31</sup> Since we are interested in the chemisorption of only one and two Mn atoms, the surface reconstruction is not taken into account in this study.

To simulate the monomer and dimer Mn adsorption, we employed a  $3 \times 3$  supercell (1/9 and 2/9 coverage) along the surface plane and considered the five layers for the Au surface slab. Due to the fact that the wave function is

expanded in plane waves, we have to consider a large empty space between periodic images perpendicular to the surface. In our calculation we took a distance of 12 Å (equivalent to five surface layers) and checked that our results did not depend on this specific value. The surface energy changes by less than 0.2% when we increase the vacuum thickness to 14 Å. Furthermore, in the calculation of the surface electronic structure and the adsorption process, the geometry was relaxed until the forces were smaller than 0.03 eV/Å. Finally, due to the metallic character of the surface, we considered a  $K$ -mesh of  $12 \times 12 \times 1$ , which allowed us to obtain a 0.01 eV accuracy in the total energy of the  $3 \times 3$  supercell.

## III. Au CLEAN SURFACE

The Au(111) surface electronic structure was obtained after a geometrical relaxation perpendicular to the surface. We present in Fig. 1 the electronic redistribution in the atoms close to the surface. Here, we plot the difference between the converged charge density of the system  $\rho_{\text{system}}$ , and the superposition of the noninteracting free atomic charge densities  $\rho_{\text{atomic}}$ ,

$$\delta\rho = \rho_{\text{atomic}} - \rho_{\text{system}}. \quad (1)$$

This function is helpful in order to visualize the electronic rearrangement due to bonding and local symmetry. In the left-hand panel we show the atoms at the surface layer. Positive values (light yellow) mean a higher electron density in the composed system as compared to the atomic distribution, and negative values (red) denote zones where the opposite occurs.

In the three right-hand panels we show the charge redistribution on planes perpendicular to the surface and passing through the various stacking lines of atoms. The first one shows a side view of the electronic redistribution on the plane that passes through the surface atoms (type A), and those on the fourth layer. One can observe that the surface atoms retain more the atomic electron configuration due to the smaller coordination and the metallic character. The next panel shows the redistribution on a plane that passes through the atoms at the second stacking layer (type B). One can notice a slight effect produced by the surface. The rightmost panel corresponds to the electronic redistribution on a plane passing through the third layer corresponding to atoms in the fcc stacking sequence of type C.

As mentioned above, the relaxation produces an expansion of 2% of the surface layer, and a compression of 0.8% of the second layer. This can be explained by noticing that the low coordination of the outermost layer produces a high attraction to the electronic cloud by the ions and a repulsion by the electronic density of the second layer (see Fig. 1).

The surface energy, defined by

$$E_s = \frac{E_{\text{system}} - N E_{\text{bulk}}}{2N}, \quad (2)$$

where  $N$  is the number of surface atoms involved, was calculated and is given in Table I, where our results are compared with previous theoretical studies, based on two different theoretical methods.<sup>32,33</sup> There is also a recent publication<sup>34</sup> in which a surface energy of 0.5 eV per atom

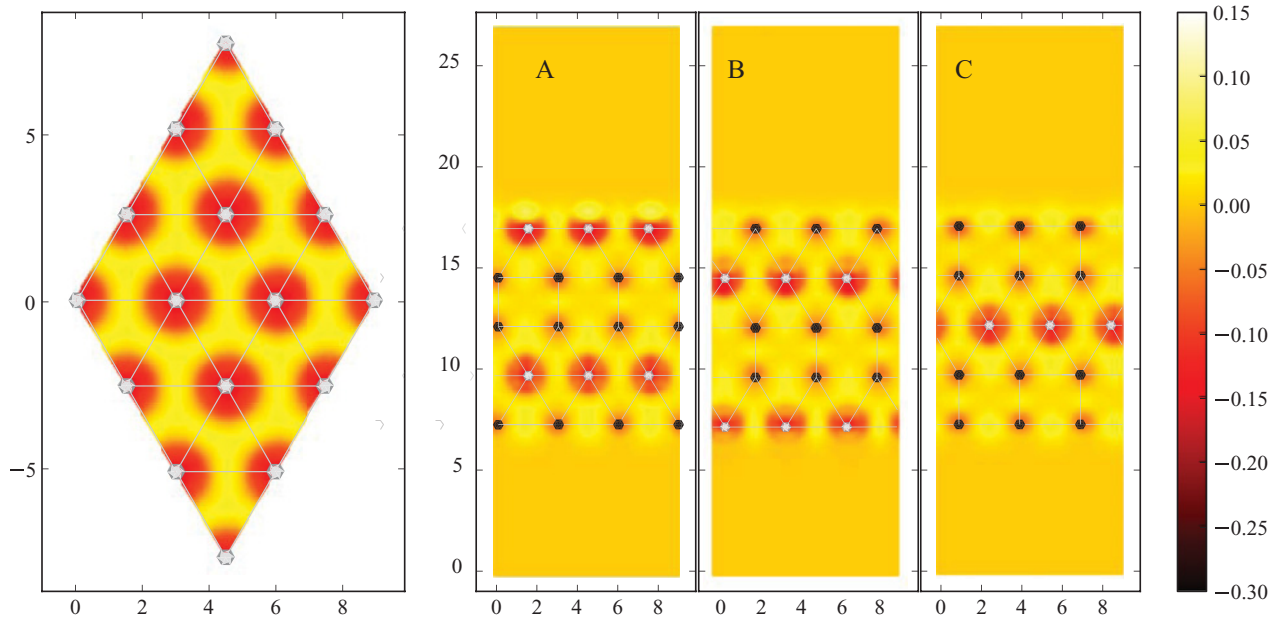


FIG. 1. (Color online) Charge redistribution  $\delta\rho$  of a Au(111) relaxed surface. The left-hand image shows the topmost surface plane passing through the relaxed surface atoms. The images A, B, C show the electronic redistribution at planes perpendicular to the surface and passing through the atoms of the three different layers (ABC fcc stacking). The distances are in  $\text{\AA}$ , and the color bar in  $e/\text{\AA}^3$ .

is reported. This value compares also well with our results (0.45 eV/atom).

The surface reconstruction of the Au(111) surface has been well characterized by diverse experimental methods.<sup>29,30,35</sup> The reconstruction consists of a periodic displacement of 46 surface atoms (two rows of 23), where close to  $2/3$  are in a fcc arrangement and  $\sim 1/3$  in hcp locations. To simulate the observed experimental reconstruction it is necessary to consider a very large ( $22 \times \sqrt{3}$ ) cell,<sup>31</sup> a calculation that demands large computational resources. We believe that this long-range atomic redistribution is not necessary to take into account in this study since our cell is much smaller than the one needed to model the reconstruction. Furthermore, it has been shown that the chemical activity of the surface is dominated by the topmost surface atoms located at fcc stacking sites.<sup>31</sup>

Although, the SOIs present in the gold atoms are not taken into account in the Mn adsorption, for the sake of completeness we calculated the surface energy including these interactions. We found that the surface energy gets increased to  $0.059 \text{ eV}/\text{\AA}^2$ , but the changes in the geometrical structure are minor; the interatomic distances differ only by  $0.001 \text{ \AA}$ . Thus, we ignore the SOI in the rest of the study. Even still, we did specific testing of the adsorption geometries by considering this correction and the adsorption energies changed by less than 5%.

TABLE I. Calculated surface energy ( $E_s$ ) in  $\text{eV}/\text{\AA}^2$  compared to published results.

$E_s$ (This work)	0.044
$E_s$ (Ref. 32)	0.055
$E_s$ (Ref. 33)	0.049

#### IV. SINGLE Mn ATOM ADSORPTION

Once the Au (111) surface had been characterized, we proceeded with the adsorption of a single Mn atom. As shown in Fig. 2, the (111) fcc surface offers four different symmetric adsorption sites: on top of a surface Au atom (A), in the bridge position between two surface Au atoms (AA), or in three coordinated sites. The three coordinated sites are of two types, one that follows the hcp sequence (B), and other that follows the fcc stacking order (C). In Fig. 2, the purple circles A, B, C, and AA denote the chemisorption sites. The first, second and third layer surface atoms are denoted as dark, medium and light gray circles, respectively. To find the equilibrium geometry, we performed an optimization of the position of both the adatom and the atoms at the three surface layers (but keeping the two further layers fixed, as before).

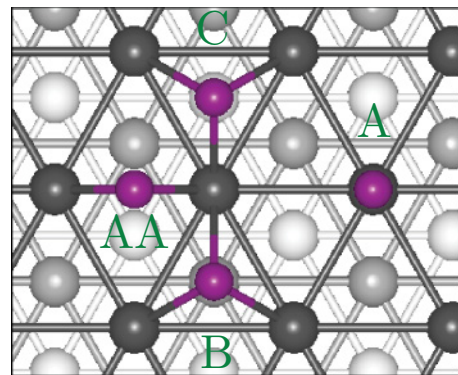


FIG. 2. (Color online) Adsorption sites on a fcc (111) surface. The site of type A is on the top of a surface atom, B and C, are above the surface and coordinated to three surface atoms, and AA is bonded to two surface atoms. The difference between B and C is that B has a Au neighbor in the second layer while C does not.

TABLE II. Adsorption energy in eV, the Mn magnetic moment in  $\mu_B$ , and the distance between the Mn atom and the surface plane ( $d_{\text{Mn-surf}}$ ) in Å.

Site	$E_A$	$\mu$	$d_{\text{Mn-surf}}$
A	-1.95	5.07	2.44
AA	-2.73	4.83	2.52
B	-2.80	4.83	2.58
C	-2.81	4.82	2.58

In this process, we allowed the relaxation of the spin degrees of freedom at the Mn atoms, and calculated the local magnetic moment by using an atomic sphere with radius 1.32 Å.

In Table II we present the results for the adsorption energy,

$$E_A = \frac{E_{\text{Tot}} - E_{\text{surf}} - N E_{\text{Mn}}}{N}, \quad (3)$$

where  $N$  is the number of adsorbed Mn atom for each of the nonequivalent adsorption sites. We also give the results for the Mn atomic magnetic moment in  $\mu_B$ , and the distance between the Mn atom and the surface plane in Å,  $d_{\text{Mn-surf}}$ .

We see that the highest adsorption energy corresponds to a chemisorption site of type C, which is the threefold coordinated site that follows the fcc gold stacking sequence. The bonding in a B site is very similar and almost degenerate to C. The magnetic moment is also very similar in both sites, 4.82 and  $4.83\mu_B$ , respectively. Furthermore, the distance from the adatom to the Au surface is the same.

The bonding energy of a Mn chemisorbed at a bridge site (AA) is smaller, as well as the distance  $d_{\text{Mn-surf}}$ , but the magnetic moment is the same as in the C case. It is important to notice that in this case, the Mn atom is bonded to two nearest neighbors on the surface and to two next-nearest neighbors in the same layer. The distance at which the nearest and

next-nearest neighbors are located differs only by a small amount, i.e., 2.52 and 2.95 Å, respectively.

The adsorption in an A site produces a large electronic localization around the Mn atom, which is probably responsible for the weakest bonding energy among all the considered sites. From these results we conclude that the adsorption of Mn clusters on gold surfaces is ruled by the Mn-surface interaction, since the bonding energies are at least four times larger than the Mn-Mn free dimer bonding energy ( $\sim 0.5$  eV). We also note that the magnetic properties are almost independent of the adsorption site, but it still holds that the lower the energy, the smaller the magnetic moment. Furthermore, the bridge type is also competitive with respect to B and C, which indicates that in the growing process, due to its dynamical dependence, the adsorption on B, C, and AA is competitive between them, and the adsorption type will depend mostly on the site surface density.

To better understand the adsorption at an electronic level, one can notice the differences at each site by plotting the difference  $\delta\rho$  between the converged charge density, including the Mn atom, and the superposition of the free atomic charge densities. From Fig. 3 one can see marked differences between the adsorption over a type A site and the other sites: The A-site adsorption affects more notoriously the Au atom below and displaces it inside the solid. One can also notice that some electrons are pulled from the surface neighbors and accumulated mainly close to the Mn and the Au atom below, and that there is a small accumulation of electronic charge on the Au surface neighbors (Mn loses on the order of  $1/4 e^-$  after adsorption, mostly from  $s$ -like orbitals).

In the B, C, and AA cases, the charge redistributions are very similar, giving rise only to small differences. In these cases the bonding is more uniform: The Mn not only shares its electrons with its nearest Au, but also does it with the metallic surface electronic cloud. This fact makes  $E_A \sim 1$  eV larger than

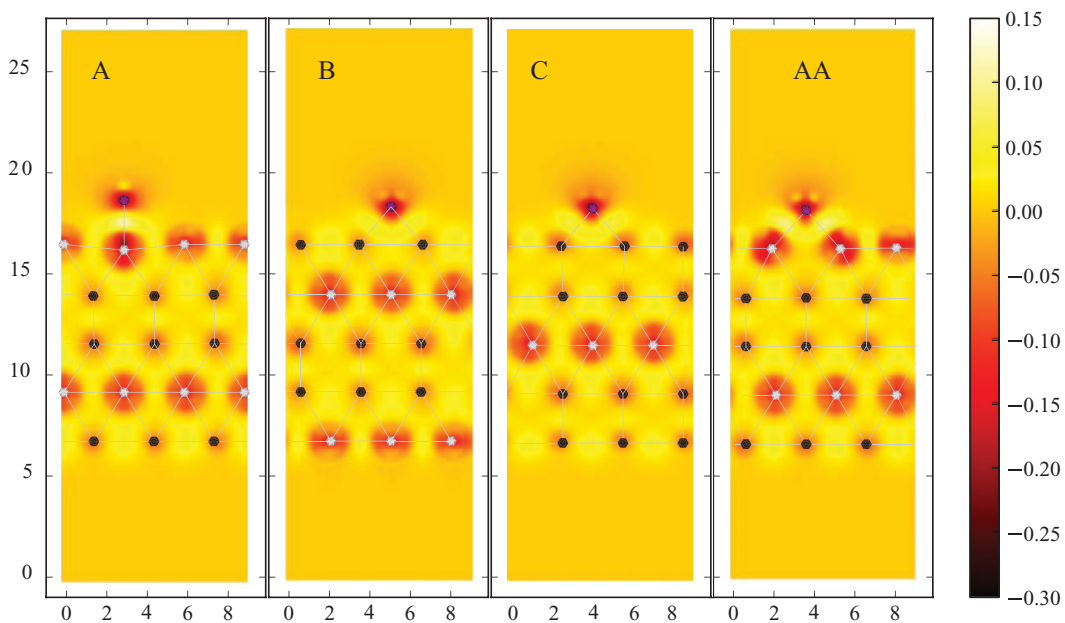


FIG. 3. (Color online) Charge redistribution  $\delta\rho$  for each adsorption site of a (111) Au surface. The red circles denote the Mn and the substrate atoms located at the same plane. The distances are in Å, and the color bar in  $e/\text{Å}^3$ .

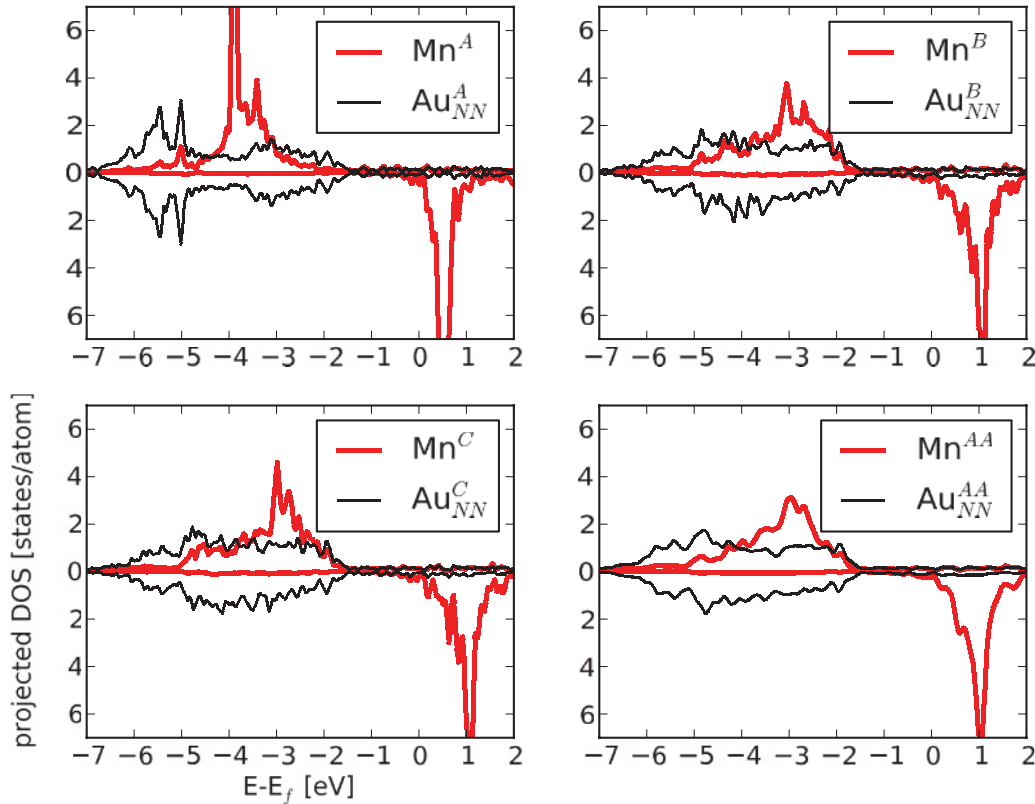


FIG. 4. (Color online) Local electronic density of states (LDOS) on Mn and on the neighbor Au (111) atoms. Each adsorption site is indicated by a superscript in the legend.  $Au_{\text{surf}}$  is the DOS of the nearest-neighbor surface Au atom. The LDOS in the lower panel corresponds to the spin-minority states.

that for the chemisorption on an A site. One can also observe that the electronic rearrangements due to the adatom has little effect in layers deeper than the second Au atomic layer.

Figure 4 shows the local electronic density of states (LDOS) for each adsorption site on the (111) Au surface. The LDOS of the surface nearest-neighbor Au atoms reflects the presence of the Mn atom. In the A case, the Au LDOS presents, in the low-energy part, peaks produced by the interaction with the Mn atom chemisorbed at the top of it. Cases B and C show only very slight differences. A more continuous DOS is obtained in the AA case, due to the higher effective coordination number. In the Au atoms, we only notice a rather small asymmetry between the up and down states, a fact that produces only small magnetic moments ( $\approx 0.05 \mu_B$  in the nearest Mn neighbors, and one order of magnitude smaller on Au second neighbors).

In contrast, the Mn LDOS presents larger differences for the various adsorption sites, although, as expected, these differences are much smaller between the B and C sites. However, the atomic character of the Mn is still clearly identified (half-filled  $d$  orbitals below  $E_F$ ). In particular, the A site yields more localized Mn  $d$  states. The LDOS around the Fermi level has few states, but a closer look (checking the orbital contributions to the electronic bands) shows that it is populated mainly with  $s$  electrons. The magnetic moment of the Mn atom has a contribution from the  $s$  electrons and yields a value of  $5.07 \mu_B$ . Furthermore, it is worth noticing that in the AA case, the interaction of the Mn atom with four atoms

(two nearest-neighbor surface atoms and two next-nearest neighbors located at the same layer) produces a LDOS with features similar to the C and B cases, but with smaller peaks. The magnetic moment values for the AA, B, and C are almost identical ( $\sim 4.83 \mu_B$ ).

## V. Mn DIMER ADSORPTION

We proceeded considering the adsorption process of a second Mn by accounting for two different cases: one where the dimer is directly adsorbed and another one where two dissociated but closely positioned atoms are placed on the surface. The presence of a gold surface adds more degrees of freedom, produced by the bond dimer orientation with respect to it and the orientation of the magnetic moments of both manganese atoms. Let us mention that from our calculation of the free Mn dimer, we obtain as a result that the two atoms are coupled antiferromagnetically, with a binding energy per atom of  $-0.53$  eV and a bond length of  $2.6 \text{ \AA}$ . The ferromagnetically ordered dimer gives the same bond length, but a weaker binding energy of  $\approx -0.28$  eV, close to previous calculations.<sup>8</sup> As mentioned above, it is worth noting that the competition between energetics and spin orientation is determined by the dimer bond length.<sup>8</sup> Even still, we do recognize that this effect remains a topic of debate.

Since the chemisorption energy of a single Mn atom is approximately four times the binding energy of the free Mn dimer, its electronic properties, once deposited on the

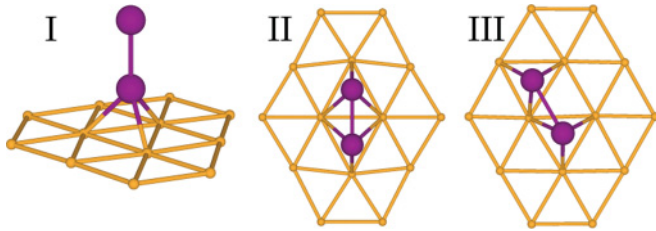


FIG. 5. (Color online) Adsorption geometries considered for  $\text{Mn}_2$  on a Au (111) surface. Site I correspond to the dimer chemisorbed, perpendicular to the surface, on a threefold coordinated site. In cases II and III the dimer is chemisorbed parallel to the surface, on nonequivalent and equivalent triangles, respectively.

surface, are ruled by the Mn-surface interaction. Thus, one must optimize all the nonequivalent geometrical and magnetic configurations.

The considered adsorption geometries for  $\text{Mn}_2$  on the Au surface are shown Fig. 5. Based on our results for a single atom adsorption, which show that the B and C sites are the most stable, we locate in one of those sites the first Mn atom. Thus, we optimize all possible configurations with one Mn atom over a B or C site and the other on a B, C, or AA site, or on top of the first Mn atom. After the optimization, the chemisorption on an AA bridge site became unstable, i.e., when an Mn atom was initially over an AA bridge, it diffuses toward a B or a C site. Similar to the monomer case, there were only slight differences between the dimer chemisorption on B and C sites. Therefore, we have considered B and C sites as equivalent. We must point out that this is a conclusion reached after the corresponding calculations and not an *a priori* approximation. We present the results only of the three geometries shown in Fig. 5. In geometry I, the dimer is chemisorbed perpendicular to the surface. Then, by fixing one of the manganese atoms on one of those positions, the other is placed either on a nonequivalent

TABLE III.  $\text{Mn}_2$  adsorption on (111) Au: The adsorption energy is in eV, the magnetic moment is in  $\mu_B$ , the Mn-Mn bond length ( $d_{\text{Mn-Mn}}$ ), and Mn-surface ( $d_{\text{Mn-surf}}$ ) distances are given in Å.

Site\Mag	$E_A$		$\mu$		$d_{\text{Mn-Mn}}$		$d_{\text{Mn-surf}}$	
	FM	AFM	FM	AFM	FM	AFM	FM	AFM
I	-3.67	-3.93	9.45	0.25	2.71	2.48	2.61	2.59
II	-5.35	-5.40	9.22	0.00	2.67	2.56	2.52	2.53
III	-5.45	-5.51	9.28	0.00	2.84	2.74	2.60	2.59

triangular site facing the first (geometry II), or on a neighbor equivalent triangular site (geometry III).

In Table III we present results for the dimer chemisorption assuming FM or AFM ordering, for the three geometries. We observe that the weakest energy of adsorption corresponds to case I, due to the fact that one of the Mn bonds to a single Au atom and the other is threefold coordinated. This geometry has also the largest energy difference between both magnetic couplings (FM and AFM). The adsorption energy for the geometries parallel to the surface differs in  $\approx 0.1$  eV for the two types of magnetic ordering. The strongest chemisorption energy corresponds to geometry III in the AFM ordering. The magnetic moment of each Mn atom in this case is  $4.64 \mu_B$ , and for the bond distance of the chemisorbed dimer we obtain  $2.74 \text{ \AA}$ , a value that is similar to the free Mn dimer.

The electronic redistribution after adsorption, for geometries I and III, is shown in Fig. 6. The two left-hand panels contain the results for geometry I assuming FM and AFM coupling. Geometry I is interesting, due the great deformation of the electron cloud in the upper Mn, which arises from sharing its valence  $s$  electron with the lower Mn. Also, site I shows a significant difference between FM and AFM states. In the two left-hand panels the corresponding results for geometry

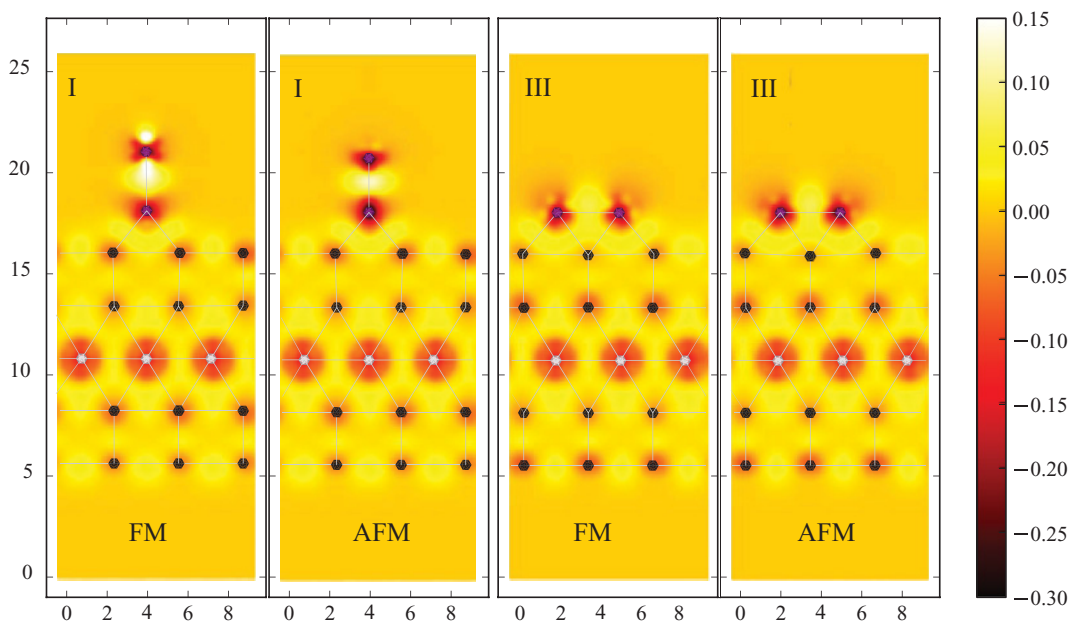


FIG. 6. (Color online) Charge redistribution of  $\text{Mn}_2$  adsorbed in (111) Au surface. The I and III geometries were minimized under two different magnetic configurations: FM and AFM ordering. The scale denotes the distance in Å and the color bar is in of  $e/\text{\AA}^3$ .

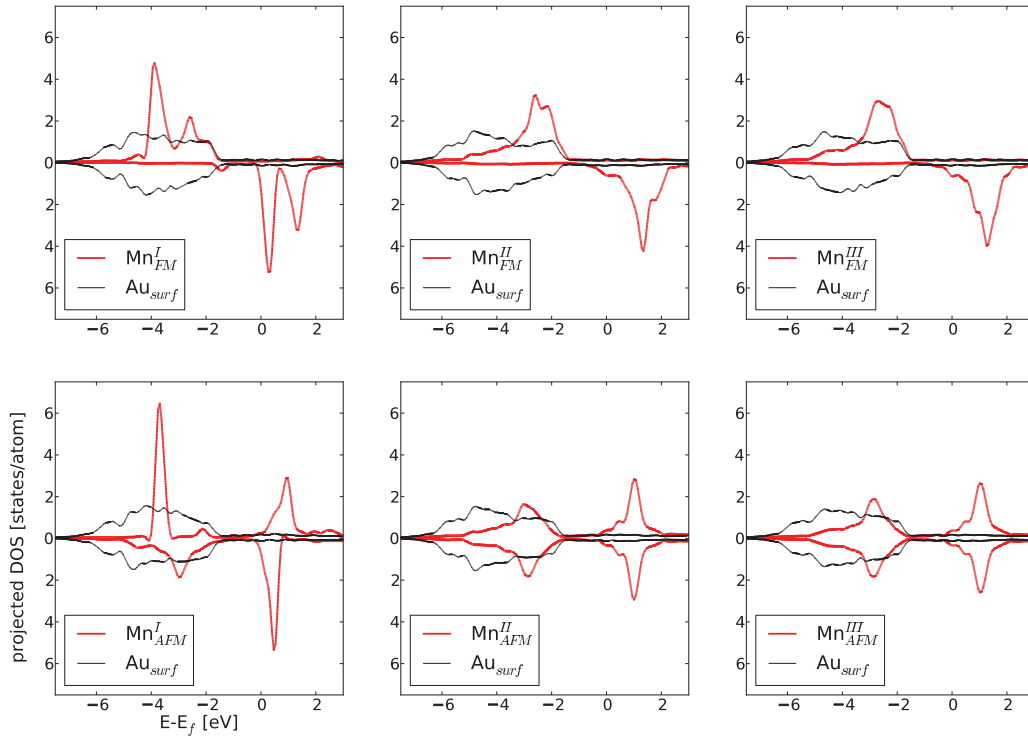


FIG. 7. (Color online) Local electronic density of states of Mn<sub>2</sub> on Au (111). The Mn superscript (in the legends) indicates the adsorption site of Mn<sub>2</sub>, and the subscript is the magnetic order considered.

III are shown. In this case the differences between the two magnetic orientations are smaller.

We report the LDOS of the chemisorbed dimer in Fig. 7. We observe that the changes in the electronic structure of the gold nearest neighbors are small and we only observe small changes around the Fermi energy. On the other hand, the

electronic DOS associated with the Mn<sub>2</sub> shows interesting features. In geometry I, where the Mn dimer is deposited perpendicular to the surface, the *e*-LDOS shows large peaks around the bonding and antibonding states of the free dimer. In geometries II and III, where the dimer lies parallel to the surface, the orbital hybridization with a larger number of gold

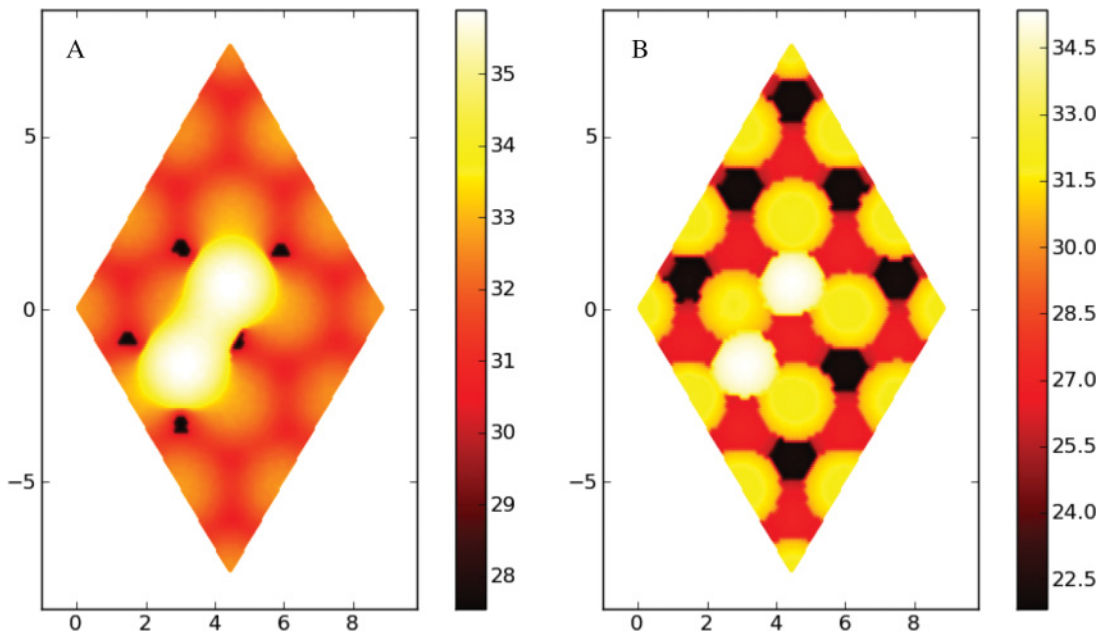


FIG. 8. (Color online) Simulated STM images for a Mn dimer chemisorbed on the most probable geometry (III) on a (111) Au surface. The applied voltage is 5.0 V and the charge density is kept constant to the values 0.1 (A) and 0.3 (B) e/Å<sup>3</sup>, respectively. The color bar indicates the depth in Å.

atoms is more important and therefore it leads to a more intense electronic dispersion. The bonding and antibonding peaks observed in case I are smoothed in these cases and become almost imperceptible. The AFM solution shows larger peaks for case I, giving a finite value for the sum of both magnetic moments. This is not the case in geometries II and III in which the two Mn are equivalent and possess equal magnetic moments of opposite sign.

Finally, we simulated STM images of the most stable dimer chemisorption geometry. Figure 8 contains the simulations in which the applied voltage was set to 5.0 V; the upper and lower figures correspond to electronic densities of 0.1 and 0.3  $e/\text{\AA}^3$ , respectively. One clearly observes the Mn dimer above the surface and the atoms lying on the surface plane. In the lower figure one can also distinguish the Au atoms of the second surface layer. These images may be useful to experimentalists studying this system. It has been shown that one can manipulate single Mn atoms adsorbed on Ag(111) to build clusters up to tetramers.<sup>36</sup>

## VI. SUMMARY AND CONCLUSIONS

We have reported a set of calculations on the monoatomic and dimer adsorption of manganese on a (111) Au surface, within the DFT theory as implemented in the VASP code. For completeness, we characterized first the bulk and the clean (111) Au surface. As a first approximation, we ignored the SOI in the gold atom basically because we found it plays a minor role in the Mn-Au interaction. Then, we calculated the binding energy of a Mn monomer and found that the strongest corresponds to the adsorption on the threefold coordinated hollow sites. We obtained a value of 4.82  $\mu_B$  for its magnetic moment.

The dimer adsorption was modeled by fixing one of the atoms to the lowest-energy configuration in the monoatomic case (threefold coordinated hollow site) and considering different geometry configurations. From those considered, we found only three different low-energy geometries. We found that the most stable configuration corresponds to the dimer lying parallel to the surface, with its atoms occupying threefold coordinated hollow sites. We found that the AFM arrangement is the most stable. The interaction with the surface modifies the value of the atomic magnetic moment, and yields 4.6  $\mu_B$  per atom. Furthermore, the dimer bond is larger than the one in the isolated dimer, but this increase is not enough to produce a FM ground state. Considering that the adsorption energy for the dimer,  $-5.51$  eV, is less than twice the adsorption energy for the monomer adsorption, one expects that the dimer will dissociate to allow the single atoms to explore the surface and bind to sites of type B or C.

Finally, we simulated STM images of the Mn dimer chemisorption. These can be useful to experimentalists working on Mn-Au systems. Investigations on the chemisorption of Mn atoms on Ag and Cu are in progress.

## ACKNOWLEDGMENTS

The authors acknowledge support from FONDECYT 1100365, the Millennium Science Nucleus Basic and Applied Magnetism P06-022-F, Financiamiento Basal para Centros Científicos y Tecnológicos de Excelencia, under project FB 0807, and CONACYT (Mexico) through Grants No. 61417 and No. 83247, and TAMU-Conacyt agreement. The use of computer resources from the Centro Nacional de Supercomputo (CNS), México is also acknowledged.

- 
- <sup>1</sup>B. Belhadji, S. Lounis, M. Benakki, and C. Demangeat, *Phys. Rev. B* **69**, 064431 (2004).
- <sup>2</sup>G. Bihlmayer, P. Kurz, and S. Blügel, *Phys. Rev. B* **62**, 4726 (2000).
- <sup>3</sup>C. Biswas, R. S. Dhaka, A. K. Shukla, and S. R. Barman, *Surf. Sci.* **601**, 609 (2007).
- <sup>4</sup>M. Hortamani, H. Wu, P. Kratzer, and M. Scheffler, *Phys. Rev. B* **74**, 205305 (2006).
- <sup>5</sup>P. Krüger, M. Taguchi, and S. Meza-Aguilar, *Phys. Rev. B* **61**, 15277 (2000).
- <sup>6</sup>O. Rader, T. Mizokawa, A. Fujimori, and A. Kimura, *Phys. Rev. B* **64**, 165414 (2001).
- <sup>7</sup>C. Demangeat and J. C. Parlebas, *Rep. Prog. Phys.* **65**, 1679 (2002).
- <sup>8</sup>J. Mejía-López, A. H. Romero, M. E. Garcia, and J. L. Morán-López, *Phys. Rev. B* **74**, 140405 (2006).
- <sup>9</sup>D. Hobbs, J. Hafner, and D. Spišák, *Phys. Rev. B* **68**, 014407 (2003).
- <sup>10</sup>M. B. Knickelbein, *Phys. Rev. Lett.* **86**, 5255 (2001).
- <sup>11</sup>J. Mejía-López, A. H. Romero, M. E. Garcia, and J. L. Morán-López, *Phys. Rev. B* **78**, 134405 (2008).
- <sup>12</sup>O. Rader, W. Gudat, C. Carbone, E. Vescovo, S. Blügel, R. Kläsger, W. Eberhardt, M. Wuttig, J. Redinger, and F. J. Himpsel, *Phys. Rev. B* **55**, 5404 (1997).
- <sup>13</sup>C. Ross, B. Schirmer, M. Wuttig, Y. Gauthier, G. Bihlmayer, and S. Blügel, *Phys. Rev. B* **57**, 2607 (1998).
- <sup>14</sup>P. Schieffer, C. Krembel, M. C. Hanf, G. Gewinner, and Y. Gauthier, *Phys. Rev. B* **62**, 2944 (2000).
- <sup>15</sup>M. Fonin, Y. Dedkov, U. Rüdiger, and G. Güntherodt, *Surf. Sci.* **529**, L275 (2003).
- <sup>16</sup>S. Uzdin, V. Uzdin, and C. Demangeat, *Surf. Sci.* **482**, 965 (2001).
- <sup>17</sup>M. Kabir, D. G. Kanhere, and A. Mookerjee, *Phys. Rev. B* **75**, 214433 (2007).
- <sup>18</sup>S. Uzdin, V. Uzdin, and C. Demangeat, *Europhys. Lett.* **47**, 556 (1999).
- <sup>19</sup>V. S. Stepanyuk, W. Hergert, K. Wildberger, S. K. Nayak, and P. Jena, *Surf. Sci.* **384**, (1997).
- <sup>20</sup>R. Martin, *Electronic Structure: Basic Theory and Practical Methods* (Cambridge University Press, Cambridge, UK, 2004).
- <sup>21</sup>G. Kresse and J. Hafner, *Phys. Rev. B* **47**, 558 (1993).
- <sup>22</sup>G. Kresse and J. Hafner, *Phys. Rev. B* **49**, 14251 (1994).
- <sup>23</sup>G. Kresse and J. Furthmüller, *J. Comput. Mater. Sci.* **6**, 15 (1996).
- <sup>24</sup>G. Kresse and J. Furthmüller, *Phys. Rev. B* **54**, 11169 (1996).
- <sup>25</sup>P. E. Blöchl, *Phys. Rev. B* **50**, 17953 (1994).
- <sup>26</sup>G. Kresse and D. Joubert, *Phys. Rev. B* **59**, 1758 (1999).
- <sup>27</sup>J. P. Perdew, K. Burke, and M. Ernzerhof, *Phys. Rev. Lett.* **77**, 3865 (1996).
- <sup>28</sup>[[http://www.webelements.com/gold/crystal\\_structure.html](http://www.webelements.com/gold/crystal_structure.html)].

- <sup>29</sup>A. R. Sandy, S. G. J. Mochrie, D. M. Zehner, K. G. Huang, and D. Gibbs, *Phys. Rev. B* **43**, 4667 (1991).
- <sup>30</sup>U. Harten, A. M. Lahee, J. P. Toennies, and Ch. Wöll, *Phys. Rev. Lett.* **54**, 2619 (1985).
- <sup>31</sup>Y. Wang, N. S. Hush, and J. R. Reimers, *Phys. Rev. B* **75**, 233416 (2007).
- <sup>32</sup>J. Wan, Y. L. Fan, D. W. Gong, S. G. Shen, and X. Q. Fan, *Modell. Simul. Mater. Sci. Eng.* **7**, 189 (1999).
- <sup>33</sup>S. M. Foiles, M. I. Baskes, and M. S. Daw, *Phys. Rev. B* **33**, 7983 (1986).
- <sup>34</sup>V. Zólyomi, L. Vitos, S. K. Kwon, and J. Kollár, *J. Phys. Condens. Matter* **21**, 095007 (2009).
- <sup>35</sup>W. Chen, V. Madhavan, T. Jamneala, and M. F. Crommie, *Phys. Rev. Lett.* **80**, 1469 (1998).
- <sup>36</sup>J. Kliewer, R. Berndt, J. Minár, and H. Ebert, *Appl. Phys. A* **82**, 63 (2006).